EXPERIMENT CMS AT THE LHC

A.A. Vorobyov, B.V. Bochin, S.A. Gets, V.L. Golovtsov, Yu.M. Ivanov, V.T. Kim, P.M. Levchenko, V.A. Murzin, V.A. Oreshkin, L.A. Schipunov, I.B. Smirnov, V.V. Sulimov, V.I. Tarakanov, L.N. Uvarov, S.A. Vavilov, S.S. Volkov, An.A. Vorobyov

1. Introduction

The observation of a particle with characteristics closely matching those predicted for the Standard Model (SM) Higgs boson was announced by the CMS and ATLAS experiments in July 4, 2012. This was a turning point for the experiments at the CERN Large Hadron Collider (LHC), especially because one of the main purposes of building the LHC and the CMS and ATLAS detectors was that of discovering the Higgs boson and understanding the origin of the electroweak symmetry breaking.

As it was officially stated at the European Physical Society conference in July 2013, the observed 125 GeV/c^2 resonance is indeed the Standard Model Higgs boson, though still many questions remain unanswered. The study of properties of the new 125 GeV/c^2 particle will constitute a new chapter of particle physics, one which will take the next decades to write.

In parallel with the Higgs boson discovery, the CMS experiment has kept expanding our knowledge of frontier particle physics with precise measurements of electroweak physics observables, and with the search for new particles and phenomena beyond the Standard Model.

The PNPI team is involved in the CMS project through a significant contribution to the design, construction, and maintenance of the Endcap Muon System. Also, PNPI physicists take part in the data analysis. This report presents a brief summary of the PNPI team activity in the CMS experiment, as well as some selected physics results published by the CMS Collaboration.

2. CMS detector

The Compact Muon Solenoid (CMS) is a collider detector (Fig. 1) designed to study physics of proton-proton collisions at the centre-of-mass energy up to 14 TeV at the full LHC luminosity [1].

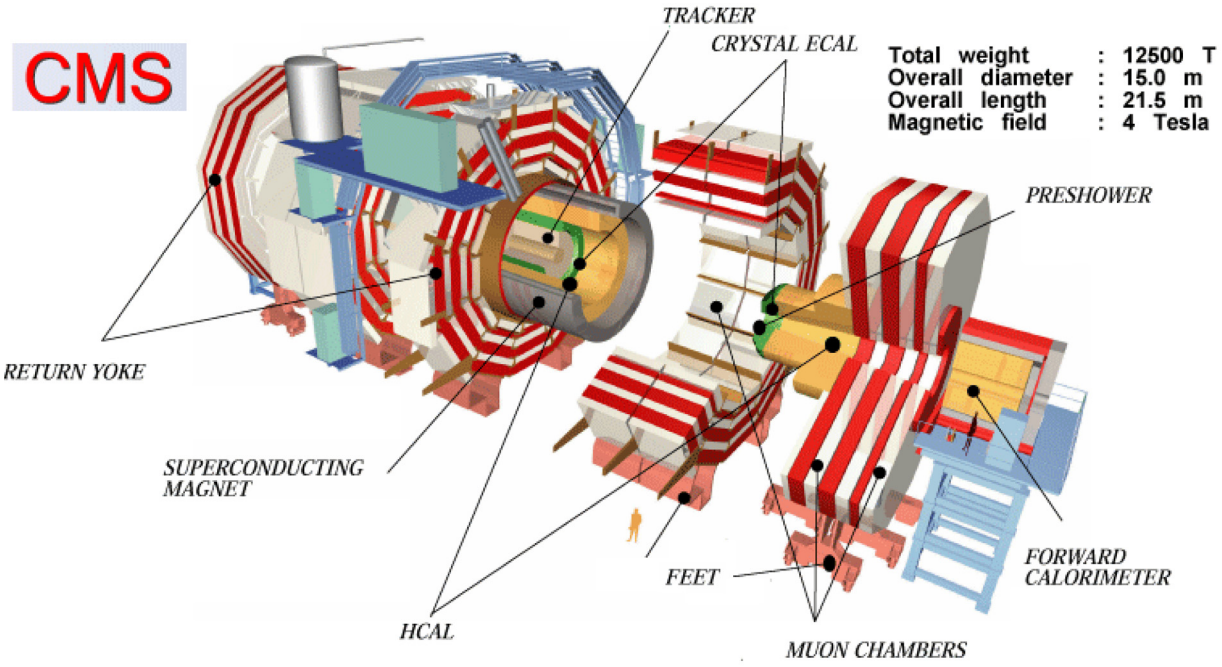

Fig. 1. Schematic view of the CMS detector

The basic element of the CMS detector is a superconducting solenoid of 6 m internal diameter, which provides a magnetic field of 3.8 T. Within the field volume, there are: the silicon pixel/strip tracker, the lead-tungsten crystal Electromagnetic CALorimeter (ECAL), and the brass/scintillator Hadron CALorimeter (HCAL). Muons are measured in gas-ionization detectors embedded in the steel flux-return yoke. The muon system consists of four stations in the barrel and in the endcap regions. Each muon station in the barrel region consists of twelve drift-tube layers, except for the outermost station, which has eight layers. In the endcap regions, each muon station consists of six planes of cathode strip chambers.

The CMS detector is operated by a collaboration of more than 4000 physicists and engineers from 182 institutions representing 42 countries. After installation and commissioning in 2007–2008, the CMS experiment started in November 2009 with the proton-proton centre-of-mass energy of 2.36 TeV and the LHC luminosity of 10^{28} $cm^{-2}s^{-1}$. By the end of 2012, after 3 years of continuous improvements, the LHC increased the *pp* centre-of-mass energy up to 8 TeV and the luminosity by more than 5 orders of magnitude up to $7.7 \cdot 10^{33}$ cm^{-2} s^{-1}. The experimental data corresponding to about 25 fb^{-1} of an integrated luminosity (about 5 fb^{-1} at 7 TeV and 20 fb^{-1} at 8 TeV, respectively) have been collected by the CMS Collaboration during this period. In February 2013, the LHC was stopped for the first Long Shutdown (LS1) for nearly two years with the goal to increase the *pp* centre-of-mass energy up to 14 TeV and to increase the luminosity up to $2 \cdot 10^{34}$ cm^{-2} s^{-1}. To optimize the performance of the CMS detector in these new conditions, the CMS Phase 1 upgrade program was launched to be implemented during LS1. A major part of this program is related with the upgrade of the Endcap Muon System.

3. PNPI participation in the design, construction, maintenance, operation, and upgrade of the CMS Endcap Muon System

3.1. Muon chambers. Status before the LS1 shutdown

The design and construction of the Endcap Muon System (EMU) was performed with an active participation of the PNPI team. Each of the two endcaps in the EMU system contains four detecting stations: ME1, ME2, ME3, ME4 (shown in red in Fig. 2). M1 station is divided into three regions: ME1/1, ME1/2, and ME1/3. The other stations are divided into two regions each: ME2,3,4/1 and ME2,3,4/2. Muons are detected with specially designed Cathode Strip Chambers (CSCs) which can measure the *r*-φ coordinates and the arrival time of each muon. The CSCs are six-plane chambers of trapezoidal shape. The cathode planes are formed by honeycomb panels with copper clad FR4 skins. Strips run radially in the endcap geometry and provide the φ-coordinate of muon hits with an accuracy of ~ 100 μm. Wires are stretched across the strips and, for readout purposes, are grouped in bunches from 5 to 16 wires. They provide the radial coordinate of the muon hits with a few cm precision.

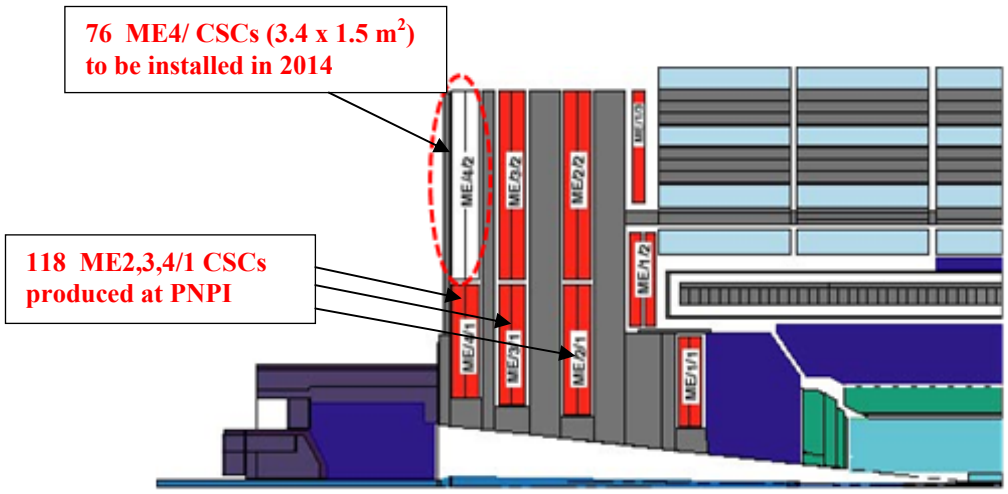

Fig. 2. Structure of the Endcap Muon System

In total, the EMU design comprised 540 CSCs, which contain 273024 cathode channels and about 2.5 million wires grouped into 210816 anode channels. However, because of finance restrictions, it was decided to postpone the construction of the ME4/2 region (72 CSCs) until the first LHC shutdown in 2013–2014.

The mass production of the chambers was distributed between three laboratories: PNPI, FNAL (USA), and IHEP (China). PNPI was responsible for assembling and testing of ME2/1, ME3/1, and ME4/1 chambers. In total, 120 CSCs (40 chambers of each type) were produced at a special facility (a muon chamber factory) prepared at PNPI to accomplish this task. The mass production of muon chambers at PNPI was started in October 2001. Full installation of these chambers in the CMS detector was completed in the end of 2007. This period of construction, testing, transportation to CERN, and installation of the CSCs is described in detail in our previous edition "HEPD Main scientific activities in 2002–2006" [2].

During the whole LHC running period in 2009–2012, the EMU system demonstrated very efficient and reliable performance even at the highest achieved luminosity $L \approx 8 \cdot 10^{33}$ cm^{-2} s^{-1}.

3.2. Muon chambers. The upgrade during LS1

The previous running period showed that the Endcap CSCs could operate without serious problems at the increased luminosity and energy planned for the running period after LS1 in 2015–2017. Therefore, a decision was taken to build CSCs for the missing station ME4/2 and to install them during the shutdown period LS1 [3]. This should considerably increase the redundancy of the Endcap Muon system. In total, 76 large area six-layers CSCs should be installed. In fact, the same type CSCs were assembled before at FNAL for stations ME2/2 and ME3/2.

Fig. 3. "Muon chamber factory" in building 904 at CERN

For several reasons, the ME4/2 chambers were to be assembled at CERN, all the materials and tooling needed for the chamber construction being supplied from FNAL. For this purpose, a "muon chamber factory" was organized in building 904 at CERN in 2011 (Fig. 3). The "factory" occupied 2000 m^2 area. It was equipped with two clean rooms, with an automated wiring machine, an automated wire soldering machine, an automated wire pitch and tension measuring machine, and with other tooling and equipment to perform chamber assembling and control on various steps of the assembling procedure.

Fig. 4. PNPI engineers played the leading role in all stages of the CSCs assembling and testing.
From left to right:
B.V. Bochin, An.A. Vorobyov, V.L. Golubev, V.V. Sulimov, S.A. Gets, V.I. Tarakanov

As a matter of fact, the ME4/2 chamber assembling technology is similar to that used earlier at PNPI to assemble ME2,3,4/1 chambers. That is why PNPI engineers (Fig. 4) were invited to participate in setting up the chamber assembling facility at CERN and to lead in production and testing ME4/2 chambers. Following the assembling of three prototype chambers for development of the assembling technology, the mass production was started in 2012. The production rate was 3 chambers per month at the initial stage. Then it was increased up to 4–5 chambers per month. The assembled chambers had to pass various controls, including gas leak tests and high voltage tests. Then they were kept under high voltage during one month, the leak currents being measured. After that, the chambers were dressed with the on-chamber electronics and tested at the cosmic muon test stand. Then they were stored under continuous gas flow expecting installation in the pit during the LS1 shutdown. This work strictly followed the production schedule according to which the production of all ME4/2 chambers should be completed by February 2014. The installation and commissioning of the chambers in the pit will be started in October 2013 with participation of the PNPI team.

3.3. High voltage system. The upgrade during LS1

The EMU CSCs require a rather complicated high voltage supply. At present, the EMU system comprises 468 six-plane muon chambers. Each plane should be provided with a high voltage line. Moreover, the HV line in each layer is subdivided into several sections (5 sections in chambers ME2/2, ME3/2 and 3 sections in all other chambers). So, in total there are more than 9000 sections with independent HV lines. This increases essentially the redundancy of the EMU system as, in case of problems, only one section will be switched off, which will not deteriorate noticeably the performance of the whole EMU system. Such a design dictated development of a special multichannel HV supply, which could satisfy the requirements of the CMS experiment. This problem was solved by joint efforts of specialists from PNPI and the University of Florida [2]. By the end of 2006, a 10000-channel HV system was designed, constructed, and delivered to CERN. The system provided independent voltage and current control in each channel. The maximal current in each channel is 100 μA. This HV system demonstrated reliable operation during all running periods in 2009–2012.

The construction of new CSCs for the ME4/2 station required additional HV supplies. The decision was to produce another 2400-channel HV system at PNPI with most of materials provided by the Florida University. The block diagram of the designed HV system is presented in Fig. 5. The high voltage from the Primary HV power supply is distributed for about 2400 HV lines with independent regulations of the voltage in each line. Also, the current in each line is under control with a possibility to switch off any line by burning off a fuse, if necessary. The HV distribution is done in two stages. Firstly, it is distributed by nine Master Boards into 72 HV lines with the HV regulation from 0 to 4 kV. These lines go *via* ~ 100 meter long cables to 72 Remote Distribution Boards. Each such board has 30 or 36 outputs going directly to the muon chambers. Including the spares, there are 96 modules to be constructed and tested: 86 Remote Distribution Boards and 10 Master Boards. The comprehensive test of the modules takes into account the requirements of the upgrade of the CMS Muon System concerning the increased LHC luminosity. The production of the 2400-channel system was started in the end of 2012, and the HV system will be finished and transported to CERN by February 2014.

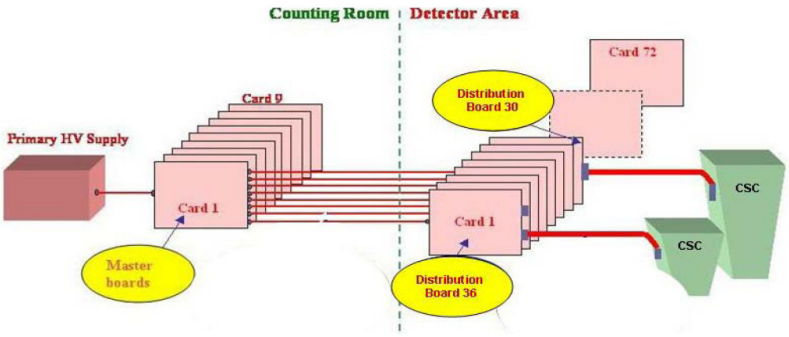

Fig. 5. Block diagram of the 2400-channel HV system

3.4. Track Finding Processor and the upgrade of the Level-1 Muon Trigger

The Track Finding Processor (TFP) is an essential part of the existing EMU trigger system. It links track segments from the individual muon stations into complete tracks, measures the transfer momentum from the sagitta induced by the magnetic bending, and reports the number and quality of the tracks to the Level-1 global trigger. The TFP (Fig. 6) was designed by PNPI engineers in cooperation with the University of Florida [2]. It is implemented as 12 processors working in parallel. Each of them should identify up to three best muons in the corresponding 60° azimuthal sectors. The design of the TFP is based on the most advanced Field Programmable Gate Array (FPGA) chips, each of them containing more than one million logical elements. The TFP was fabricated in the US industry, while testing and commissioning of this system was done by PNPI engineers in cooperation with specialists from the University of Florida. The TFP demonstrated reliable performance during the 2009–2012 running periods.

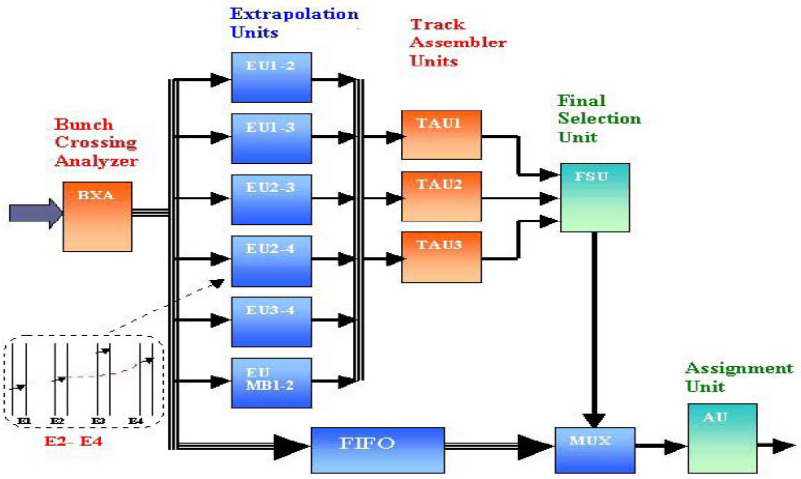

Fig. 6. Block diagram of the Track Finding Processor

The global Level-1 Muon Trigger operated with the required high efficiency in 2009–2012. However, the envisaged further increase of the LHC beam energy and luminosity creates serious problems for the trigger system. Therefore, the upgrade of the trigger system is considered as the most important part of the CMS upgrade program. For that reason, the CMS Collaboration has prepared a Technical Design Report [4] with a conceptual design of an improved muon trigger system able to select interesting collisions in this new high intensity regime.

The overall strategy is to merge the detector information from different muon sub-detector systems at the input to the muon track-finder and to form a combined track-finder layer. This substantial change to the design of the muon trigger is planned to proceed through several stages, so that commissioning of the upgrade can proceed in parallel with the running current trigger. The first step is to make several changes to the data links providing muon trigger data. The next step is to deploy the new Muon Track Finder that will be partitioned into barrel, endcap, and overlap regions. It will be commissioned in parallel with the running current trigger in 2015 using the full set of parallel inputs from the CSC and RPC systems and a subset of duplicated inputs from the DT system. The algorithms developed initially will be similar to the current trigger, but will be expanded over time to fully replace the separate CSC, DT, and RPC trigger systems. After the track-finder layer, a further layer is necessary to merge and remove duplicate muon candidates from the different track finders and also to sort the muons. The Global Muon Trigger will also be upgraded to receive more muon candidates.

The successful collaboration between PNPI and the University of Florida on the first generation muon trigger has resulted in the development of the Track-Finding Processor, which served CMS well for the first LHC runs. The PNPI team will participate also in the Muon Trigger upgrade with the responsibility to design and build the new Barrel/Endcap Overlap Track-Finding Processor.

4. Selected physics results

4.1. Search for the Higgs boson

In July 4, 2012, CMS jointly with ATLAS announced [5] that a new particle with the mass $m \approx 125$ GeV/c^2 was observed with characteristics compatible with those expected for the Standard Model Higgs boson. It was detected in its decays to bosons (photon pairs, *WW*- and *ZZ*-pairs) using 5.1 fb^{-1} at $\sqrt{s} = 7$ TeV and 5 fb^{-1} at $\sqrt{s} = 8$ TeV, respectively. The next updates [6–10], were presented in November and December 2012, and in March and May 2013, and at the European Physical Society (EPS) conference in July 2013. These results were based on 19.6 fb^{-1} at $\sqrt{s} = 8$ TeV. Also, they included decays to fermions: $\tau\tau$- and $b\bar{b}$-pairs. At the EPS conference, the new 125 GeV/c^2 resonance was officially established as the SM Higgs boson.

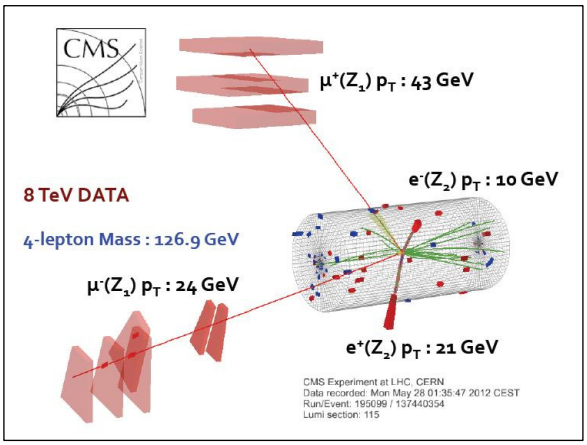

Fig. 7. Four-leptons event, a candidate for the Higgs boson decay with a mass 126.9 GeV/c^2. One of the muons is detected by the Endcap Muon System

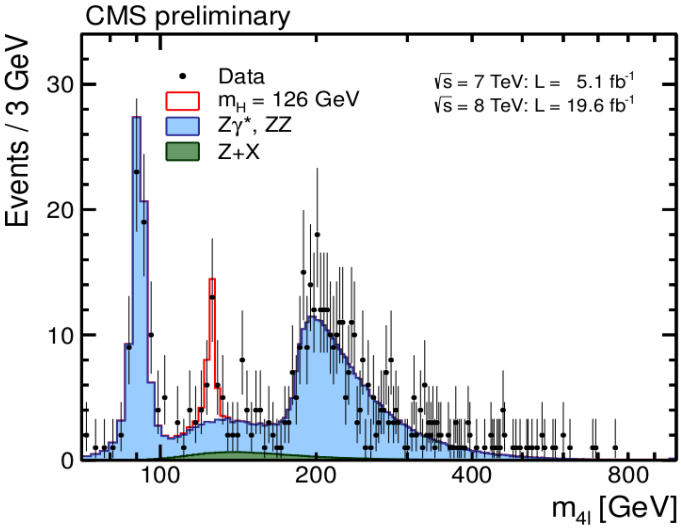

Fig. 8. Four-leptons mass distribution

The Standard Model predicted the Higgs boson existence with its mass between 115 GeV/c^2 and 140 GeV/c^2. Also, the SM predicted the production cross sections for the Higgs boson in *pp*-collisions and the branching ratios of the Higgs boson decay to various channels. The search for the Higgs boson in the CMS experiment was driven by these predictions. The cleanest signal of the Higgs boson was observed in the four-leptons decay modes, though the branching ratios to these channels are very small: Br ($H \rightarrow ZZ^* \rightarrow 4l$) $\approx 10^{-4}$ for a 125 GeV/c^2 Higgs (here, l = μ, e). Figure 7 shows one condidate for the four-leptons Higgs decay observed in the CMS experiment, and Fig. 8 presents the four-leptons mass distribution with full statistics collected by CMS. It was concluded from an analysis of this spectrum that a new particle with the mass $m_H = 125.6 \pm 0.5$ (stat.) $\pm$ 0.2 (syst.) GeV/c^2 is observed with the local significance of 6.8 standard deviations above the expected background. The width of the observed resonance was determined as $\Gamma \leq 3.4$ GeV/c^2 at the 95% CL. The signal strength μ, relative to the expectation for the Standard Model Higgs boson, is found to be $\mu = 0.91 + 0.30 - 0.24$ at the measured mass.

The $H \rightarrow \gamma\gamma$ decay is one of the most sensitive channels for the Higgs search in the mass region around 125 GeV/c^2 due to its relatively high expected branching fraction of the order of ~ 0.2 %. However, a serious problem in this case is the background. The search results were based on the Multi-Variate-Analysis (MVA) techniques for both photon identification and event classification which extracts the signal from the background using a fit to the diphoton mass spectrum shown in Fig. 9. The following results were obtained from that analysis: $m_H = 125.4 \pm 0.5$ (stat.) $\pm$ 0.6 (syst.) GeV/c^2, $\mu = 0.78 + 0.28 - 0.26$. The local significance of the observed peak at 125.4 GeV/c^2 is 3.2 standard deviations above the background.

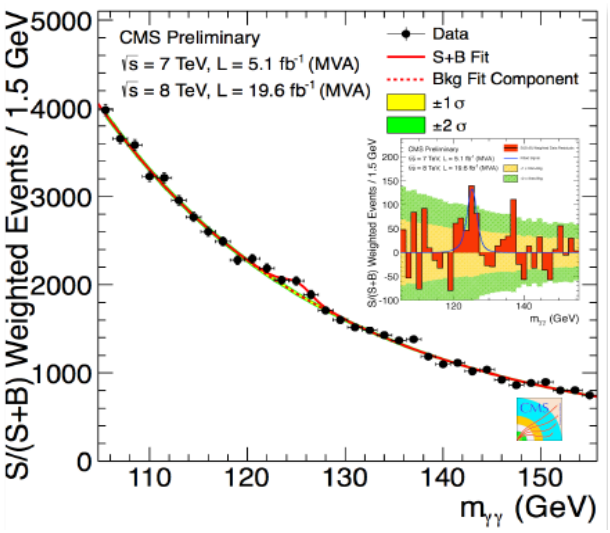

Fig. 9. Two-gammas mass distribution measured in the CMS experiment

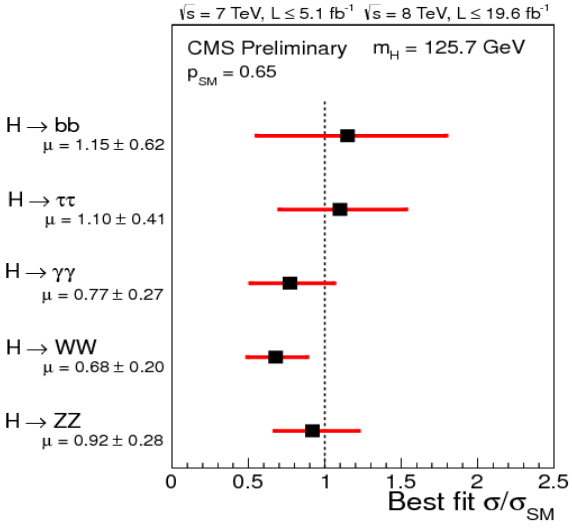

Fig. 10. Ratio of the measured yields in various decay channels of the Higgs boson to those predicted by the Standard Model

Besides the observation of the Higgs boson *via* channels $H \to ZZ^* \to 4l$ and $H \to \gamma\gamma$, the CMS Collaboration has reported also on observation of Higgs signals in $H \to WW$, $H \to bb$, and $H \to \tau\tau$ channels with the signal strengths compatible with those predicted by the Standard Model (Fig. 10). These observations are of special importance as they provide control of the SM predictions [11] both in vector boson and fermion couplings (Fig. 11).

The spin-parity of the SM Higgs boson should be 0^+ (that is it is a scalar particle). Spin 1 is excluded by the fact that the observed particle decays into two gammas. The analysis of the angular distributions of the four leptons showed that the pure scalar hypothesis is consistent with the observation when compared to six other spin-parity hypotheses. The data disfavour the pure pseudoscalar hypothesis 0^- with a CLs value of 0.16 % (Fig. 12) and disfavour the pure spin 2 hypothesis of a narrow resonance with minimal couplings to the vector bosons with a CLs value of 1.5 %.

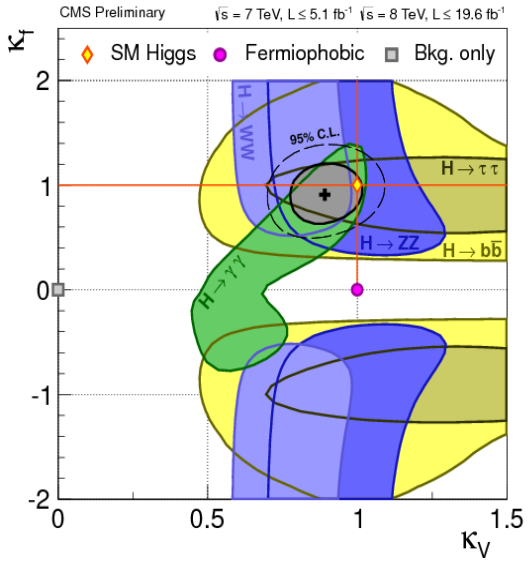

Fig. 11. The measured fermion and boson couplings in the observed channels

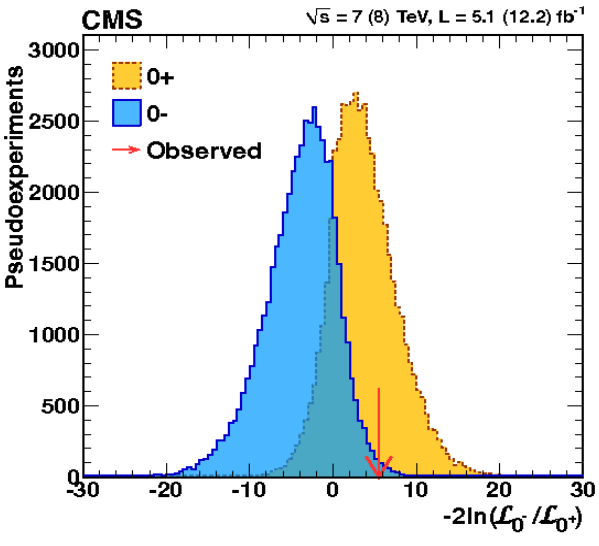

Fig. 12. Spin-parity properties: expected distribution of $-2 \cdot \ln(L0^- / L0^+)$ under the pure pseudoscalar and scalar hypotheses; the red arrow shows the observed value

To summarize, the new discovered 125 GeV/c^2 particle is compatible with the SM Higgs boson properties. It is seen beyond doubts in three boson decay channels. Fermionic decays in $b\bar{b}$ - and ττ-channels are observed, and they are in agreement within the uncertainties with the SM predictions. The two high-resolution modes allowed independent determinations of the Higgs boson mass: m_H = (125.8 ± 0.6) GeV/c^2 in $H \to ZZ \to 4l$ and m_H = (125.4 ± 0.8) GeV/c^2 in $H \to \gamma\gamma$. There is no evidence for non-SM decays and for additional Higgs bosons at higher or lower masses. ***The observed spin-parity properties and the measured couplings allow to establish the observed particle as the SM Higgs boson.***

4.2. Search for "new physics". Rare decays $B_s \to \mu^+\mu^-$ and $B_d \to \mu^+\mu^-$

The search for "new physics" beyond the Standard Model was among the main goals of the CMS experiment. One way was to make an attempt to see directly new particles (sypersymmetric partners, heavy bosons, leptoquarks, *etc*.) produced in *pp* collisions at the LHC. Various channels were tested where these new particles could be produced. However, the result was negative. So, the conclusion was that the mass of these particles (if they exist) should be higher than ~ 1 TeV/c^2. A hope still remains that such particles could be discovered in the next runs when the energy of the LHC will be increased to $\sqrt{s}$ = 14 TeV.

Another (inderect) way to see the presence of "new physics" was studies of rare decays of B mesons. From this point of view, the most promising was the decay of B_s and B_d mesons to two muons. The Standard Model predicts very low branching fractions for these decays:

$$\mathcal{B}(B_s \to \mu^+\mu^-) = (3.2 \pm 0.2) \times 10^{-9}, \quad \mathcal{B}(B_d \to \mu^+\mu^-) = (1.0 \pm 0.1) \times 10^{-10}.$$

On the other hand, "new physics" (in particular, some supersymmetric models) could drastically increase probabilities of these decays. That is why investigation of these decays attracted so much attention in the LHC experiments (LHCb and CMS). The CMS Collaboration presented results of a search for the rare decays $B_s \to \mu^+\mu^-$ and $B_d \to \mu^+\mu^-$ in *pp* collisions at $\sqrt{s}$ = 7 TeV and $\sqrt{s}$ = 8 TeV based on data samples corresponding to integrated luminosities of 5 fb^{-1} and 20 fb^{-1}, respectively [12]. An excess of $B_s \to \mu^+\mu^-$ decays was observed above the background predictions (Fig. 13).

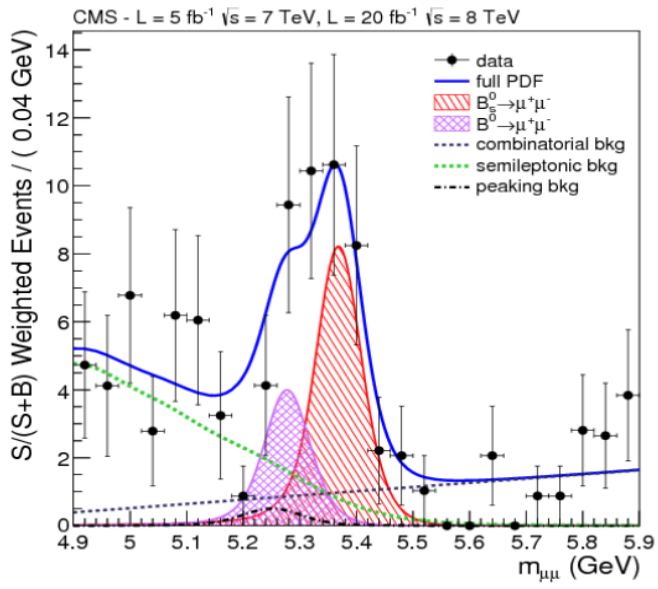

Fig. 13. Dimuon weighted mass distribution

The measured decay-time integrated branching fraction from the fit is

$$\mathcal{B}(B_s \to \mu^+\mu^-) = (3.0 + 1.0 - 0.9) \times 10^{-9},$$

where the uncertainty includes both the statistical and systematic components, but is dominated by the statistical uncertainties. The significance of the observed decay is 4.7 standard deviations. The measured branching fraction is consistent with the expectation from the SM. No excess is observed for $B_d \to \mu^+\mu^-$, with the upper limit

$$\mathcal{B}(B_d \to \mu^+\mu^-) < 1.1 \times 10^{-9}$$

at the 95 % confidence level.

Similar results were obtained in the LHCb experiment (see a special article in this edition). The fact that the measured $\mathcal{B}(B_s \to \mu^+\mu^-)$ corresponds to the SM prediction puts strong limitations for proposed models of "new physics". In particular, it excludes some of the supersymmetric models.

4.3. Ridge effect in *pp*-, *pA*- and *AA*-collisions

The first groundbreaking result at the LHC was announced by the CMS Collaboration in 2010 with the observation of long-range near-side angular correlations in *pp* collisions with high multiplicities at $\sqrt{s}$ = 7 TeV [13]. The CMS has measured the two-particle correlation function in azimuthal and pseudorapidity two-dimensional space. In high multiplicity events (N > 110), a pronounced structure ("ridge") emerges in the two-dimensional correlation function for particle pairs with intermediate p_T-values of 1–3 GeV/c, 2.0 < |Δη| < 4.8, and Δφ ≈ 0 (Fig. 14). This was the first observation of such a long-range, near-side feature in two-particle correlation functions in hadron-hadron collisions. Such a correlation was observed earlier in central heavy-ion collisions at RHIC (BNL). The heavy-ion ridge effect found at RHIC at $\sqrt{s_{NN}}$ = 0.2 TeV was interpreted as a manifestation of formation of a new state of the superdense hot nuclear matter and, hence, it should not be observed in *pp* collisions. Later, the ridge effect was observed at the LHC also in *pA*- ($\sqrt{s_{NN}}$ = 5.02 TeV) and *AA*- ($\sqrt{s_{NN}}$ = 2.76 TeV) collisions (Fig. 14). The interpretation of the ridge effect is still under discussion, and it requires further theoretical and experimental studies to test numerious models [14].

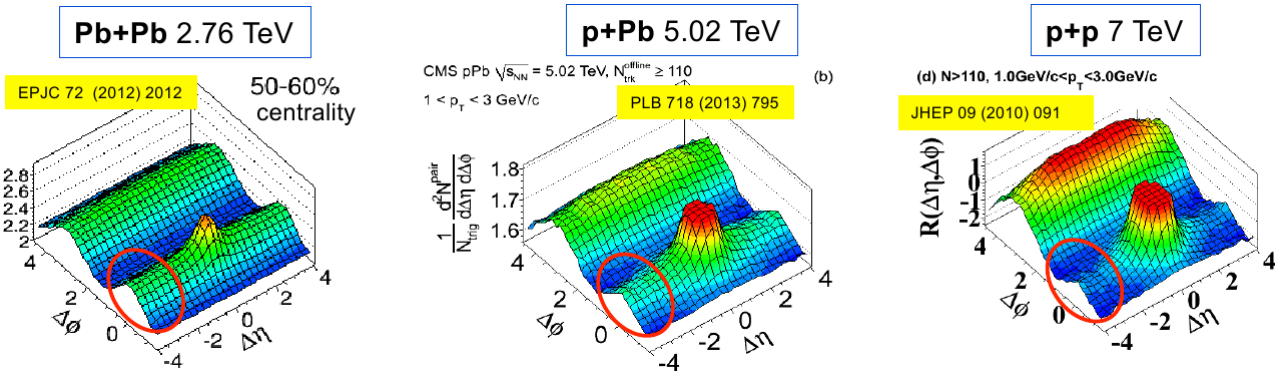

Fig. 14. Two-particle correlation functions versus Δη and Δφ for *pp*-, *pA*- and *AA*-collisions at the CMS. The cycles show the locations of the near-side ridge structures

4.4. Search for electroweak production of *Z* bosons with two forward-backward jets

The CMS has performed the first measurement of the electroweak production cross section of a Z boson with two forward jets (Zjj) in *pp* collisions at $\sqrt{s}$ = 7 TeV with an integrated luminosity of 5 fb^{-1} [15]. This process was studied in the context of rapidity intervals in hadron collisions as a probe of anomalous triple-gauge-boson couplings and as a background to Higgs boson searches in Vector Boson Fusion (VBF) processes. There are three classes of diagrams to be considered in the EW production of W and Z bosons with two forward jets: VBF processes, bremsstrahlung, and multiperipheral processes (Fig. 15). A full calculation reveals a large negative interference between the pure VBF process and the other two categories.

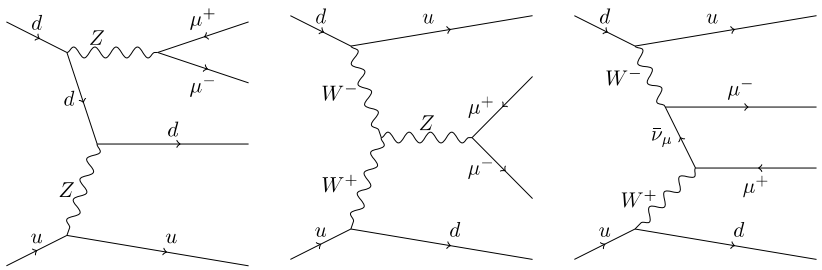

Fig. 15. Representative Feynman diagrams for electroweak *llqq'* production processes. Bremstrahlung (left); vector boson fusion (centre); peripheral (right)

The VBF Higgs boson production in *pp* collisions at the LHC has been extensively investigated as a way to discover the Higgs boson and to measure its couplings. Recent searches by the ATLAS and CMS Collaborations for the SM Higgs boson include analyses of the VBF final states. In particular, the study of the processes shown in Fig. 15 can improve our understanding of selection of the tagging jets, as well as that of vetoing additional parton radiation between forward-backward jets in VBF searches. The measurement of the electroweak production of the *Zjj* final state is also a precursor to the measurement of elastic vector boson pair scattering at high energy, an important physics goal for future analyses of LHC data.

The cross section is measured for the *lljj* ($l = e$, μ) final state in the kinematic region $m_{ll} > 50$ GeV/c^2, forward dijet $m_{jj} > 120$ GeV/c^2, jet transverse momenta $p_T > 25$ GeV/c, and the jet pseudorapidity $|\eta| < 4.0$. This measurement, combining the muon and electron channels, yields σ = (154 ± 24 (stat.) ± 46 (exp. syst.) ± 27 (th. syst.) ± 3 (lum.)) fb, in agreement with the SM prediction (~ 166 fb) for the cross section. The hadronic activity in the rapidity interval between the jets is also measured. A significance of 2.6 standard deviations has been obtained for the observation of EW production of the *Z* boson with two tagging jets. This first measurement of the *Z* boson with two jets at the hadron collider by the CMS constitutes an important foundation for a more general study of vector boson fusion processes of relevance for Higgs boson searches and for measurements of electroweak gauge couplings and vector-boson scattering.

4.5. Search for BFKL effects in forward jets

Measurements of inclusive jet production in *pp* collisions provide an important testing ground for the Standard Model. At the LHC energies, the inclusive production of jets with large transverse momentum in the central rapidity region is well described by the perturbative quantum chromodynamics (QCD) using the Gribov – Lipatov – Altarelli – Parisi – Dokshitzer (GLAPD) evolution. However, the dominant kinematical regime for jet production at the LHC energies is extended for a very wide rapidity domain. At very high energies, this dominant kinematic regime is expected to be described by the Balitsky – Fadin – Kuraev – Lipatov (BFKL) evolution [16, 17]. The BFKL-effects may dominate for the QCD background in searches for new heavy extra-dimension gravitons with forward dijets at the LHC [18, 19].

The results presented below illustrate attempts to see some evidence of the BFKL effects already at the LHC energies. For these studies, the dijet events were chosen. The events were classified as follows. The events with at least one pair of jets with $p_T > p_T^{min}$ are denoted as "inclusive". The inclusive dijets with the jets most forward and backward in the rapidity, *i.e.*, dijets with the maximal rapidity separation between the jets, are the so called Mueller – Navelet (MN) jets. Events with exactly one pair of jets with $p_T > p_T^{min}$ are called "exclusive". The ratio of the dijet production cross section for "inclusive" events to that for "exclusive" events, $R^{incl} = \sigma^{incl} / \sigma^{excl}$ (the dijet "*K*-factor"), as a function of the rapidity separation $|\Delta y|$ between two jets, may be a sensitive probe of BFKL-effects [20]. Analogously, one can consider the ratio $R^{MN} = \sigma^{MN} / \sigma^{excl}$.

The CMS performed the first measurement of the ratios R^{incl} and R^{MN} in a wide range of the rapidity separation, up to $|\Delta y| = 9.2$, in *pp* collisions at $\sqrt{s} = 7$ TeV [21]. A dedicated forward dijet trigger allowed to enhance the registration rate of the dijets by a factor of ~ 150 in the forward region. The results are shown in Fig. 16. A moderate rise of the ratios R^{incl} and R^{MN} as a function of $|\Delta y|$ is observed. In comparisons of theoretical values of R^{incl} and R^{MN} with the experimental data, three GLAPD based MC event generators were used: PYTHIA6, PYTHIA8, and HERWIG++, improved by polar angle ordering (*i.e.*, by colour coherence effects) in the parton shower. The predictions of the PYTHIA6 and PYTHIA8 generators agree with the measurements, while the predictions of the HERWIG++ generator are larger than the measurements, especially at large $|\Delta y|$ values. The BFKL-motivated generators in the leading logarithm (LL) approximation, CASCADE and HEJ+ARIADNE, predict for these ratios a significantly stronger rise than the observed one. The moderate rise of the measured dijet ratios indicates that either the BFKL effects are not dominant for jets with $p_T > p_T^{min} = 35$ GeV/c at the collision energy $\sqrt{s} = 7$ TeV, or the BFKL effects are canceled in the ratios.

There is another way to study the dynamics of hadron jets in *pp* collisions, which yields important information about underlying partonic processes. The azimuthal decorrelation of jets with a large rapidity separation might show effects beyond the GLAPD description. In the kinematic region where BFKL-effects are important, the azimuthal angle decorrelations will increase with the rapidity separation increasing.

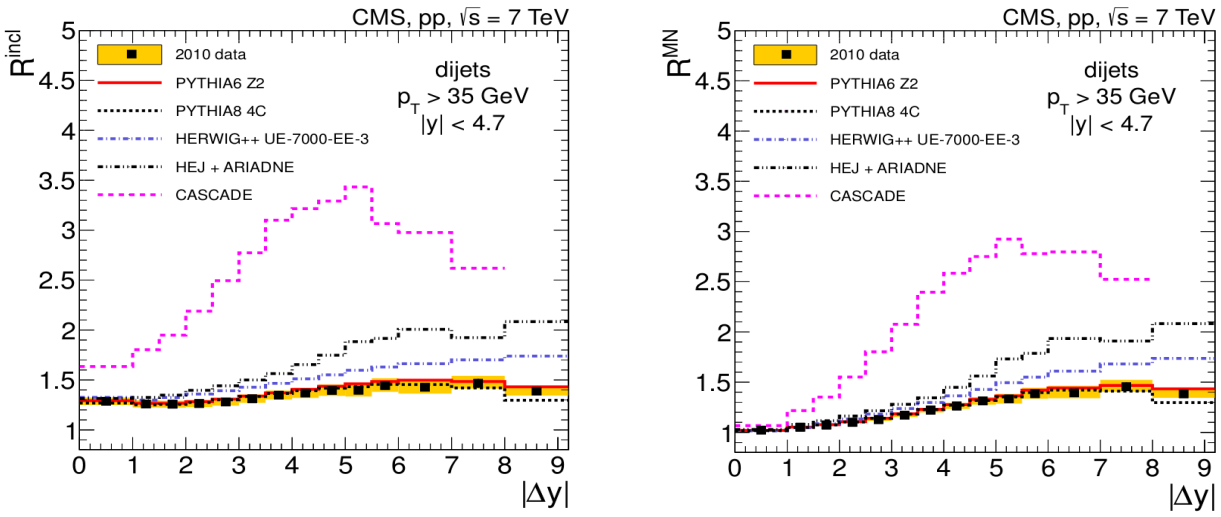

Fig. 16. First measurement of dijet raios $R^{\mathrm{incl}} = \sigma^{\mathrm{incl}}/\sigma^{\mathrm{excl}}$ (left) and $R^{\mathrm{MN}} = \sigma^{\mathrm{MN}}/\sigma^{\mathrm{excl}}$ (right) as a function of the rapidity separation between jets up to $|\Delta y| = 9.2$ at the LHC [20]

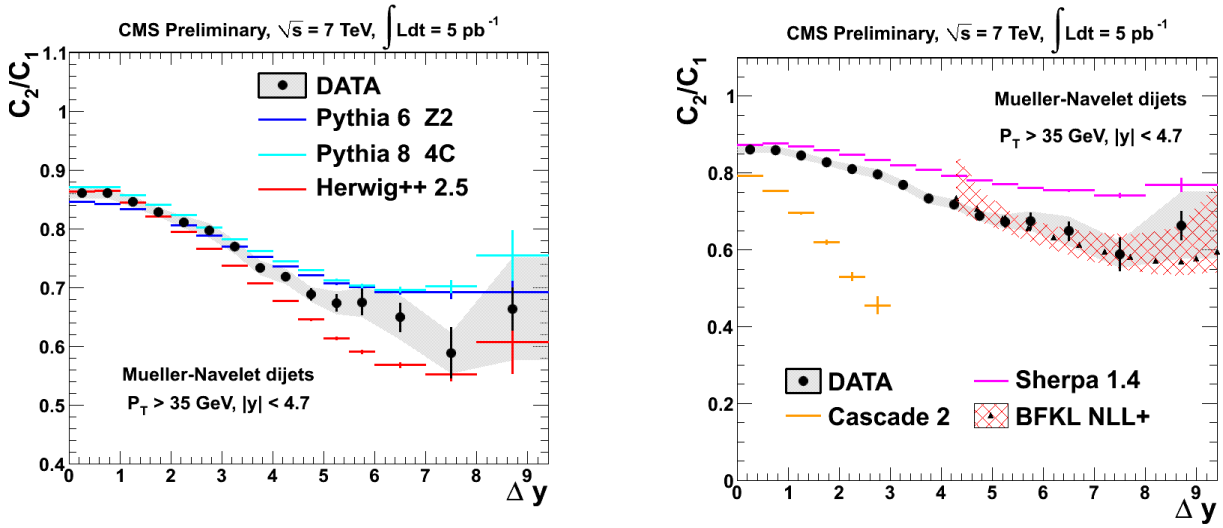

Fig. 17. First measurement of the azimuthal angle decorrelations at *pp* collisions as a function of the rapidity separation between jets up to $|\Delta y| = 9.4$ in CMS at the LHC. The ratio of average cosines $C_2 / C_1 = \langle\cos(2(\pi - \Delta\varphi))\rangle / \langle\cos(\pi - \Delta\varphi)\rangle$ is shown *vs* GLAPD MC generators (left) and *vs* BFKL predictions (right)

The first measurement of the azimuthal angle decorrelations of Mueller – Navelet dijets with a rapidity separation of up to $\Delta y = 9.4$, in proton-proton collisions at $\sqrt{s} = 7$ TeV, was performed by CMS [22]. The results are presented in Fig. 17. The average cosine ratios are particularly sensitive to details of parton showering and multiparton interaction: without implementing polar angle ordering in parton showering and multiparton interactions the considered GLAPD MC generators show significant deviations from the data. CASCADE 2, which incorporates essential elements of LL BFKL but is missing some elements of collinear factorization of the GLAPD approach, predicts too strong azimuthal decorrelations. Analytical BFKL calculations [23] performed at the next-to-leading logarithmic (NLL) approximation [24] provide a satisfactory description of the data for the average cosine ratios. The observed disagreement of the LL GLAPD MC generators without the polar angle ordering in parton showering may be considered as a hint that the kinematical domain of the present study lies in the transition between the regions described by the GLAPD and BFKL approaches. For further investigations of possible manifestations of BFKL effects, data at higher energies are needed.

5. Summary

The CMS experiment, one of the most ambitious projects in fundamental particle physics, has demonstrated at the first stage of the LHC running its extraordinary capabilities to extend the high-energy physics frontier. The main result so far is the discovery of the 125 GeV/c^2 Higgs boson, a quantum of the scalar fundamental vacuum field, which is responsible for spontaneous symmetry breaking of electroweak forces and the particle mass origin. In addition, the CMS experiment performed a large number of new precise measurements of the Standard Model physics observables, and also measurements aimed to discover new particles and phenomena beyond the Standard Model. These measurements proved to be a strong confirmation of the Standard Model with no indication of signs of "new physics" in the investigated mass region up to ~ 1 TeV/c^2.

The PNPI team has made a significant contribution to the design, construction and maintenance of the Endcap Muon System of the CMS detector. At present, the PNPI team is actively involved in the upgrade of the Endcap Muon System of the CMS detector for the challenging high luminosity beam conditions at the next stage of the LHC operation. PNPI physicists have contributed to the CMS data analysis, in particular in searches for the Higgs boson in vector boson fusion production, in studies of the electroweak *Z*-boson production with forward jets, and for BFKL physics in forward dijets as a novel QCD dynamics in a new energy domain.

In total, the CMS Collaboration has published 242 physics papers in the period 2010 – July 2013. The list of authors in the CMS physics publications includes PNPI physicists and engineers: A.A. Vorobyev, Yu.M. Ivanov, V.L. Golovtsov, V.T. Kim, P.M. Levtchenko, V.A. Murzin, V.A. Oreshkin, I.B. Smirnov, V.V. Sulimov, L.N. Uvarov, S.A. Vavilov, An.A. Vorobyev.

References

1. CMS Collaboration, JINST **3**, S08004 (2008).
2. A.A. Vorobyov *et al.*, PNPI HEPD Main Scientific Activities, 2002–2006, PNPI, 2007, pp. 26–34.
3. CMS Collaboration, CMS U1 TDR, June 2011.
4. CMS Collaboration, CERN-LHCC-2013-011, CMS-TDR-012, June 2013.
5. CMS Collaboration, Phys. Lett. B **716**, 30 (2012).
6. CMS Collaboration, CMS-PAS-HIG-13-002, March 2013.
7. CMS Collaboration, JHEP **06**, 081 **(**2013).
8. CMS Collaboration, Phys. Rev. Lett. **110**, 081803 (2013).
9. CMS Collaboration, CMS-PAS-HIG-13-016, July 2013.
10. CMS Collaboration, CMS-PAS-HIG-13-005, April 2013.
11. V.T. Kim, Nucl. Phys. Proc. Suppl. **198**, 223 (2010).
12. CMS Collaboration, Phys. Rev. Lett. **111**, 101804 (2013).
13. CMS Collaboration, JHEP **1009**, 091 (2010).
14. I.M. Dremin and V.T. Kim, Pis'ma ZhETF **92**, 720 (2010) [JETP Lett. **92**, 652 (2010)].
15. CMS Collaboration, CMS-PAS-FSQ-12-019, November 2012, JHEP (2013), in press.
16. E.A. Kuraev, L.N. Lipatov, and V.S. Fadin, ZhETF **72**, 377 (1977) [JETP **45**, 199 (1977)].
17. I.I. Balitsky and L.N. Lipatov, Yad. Fiz. **28**, 1597 (1978) [Sov. J. Nucl. Phys. **28**, 822 (1978)].
18. V.T. Kim *et al*. Nucl. Phys. Proc. Suppl. **198**, 220 (2010).
19. V.T. Kim and V.A. Oreshkin, Nucl. Phys. Proc. Suppl. **219–220**, 235 (2011).
20. V.T. Kim and G.B. Pivovarov, Phys. Rev. D **53**, 6 (1996).
21. CMS Collaboration, Eur. Phys. J. C **72**, 2216 (2012).
22. CMS Collaboration, CMS-PAS-FSQ-12-002, April 2013.
23. S.J. Brodsky *et al*., Pis'ma ZhETF **70**, 161 (1999) [JETP Lett. **70**, 155 (1999)].
24. B. Ducloue, L. Szymanowski, and S. Wallon, JHEP **1305**, 096 (2013).